Mech. Sci., 2, 129–137, 2011
www.mech-sci.net/2/129/2011/
doi:10.5194/ms-2-129-2011

Mechanical Sciences
Open Access

Fabrication of compliant mechanisms on the mesoscale

G. R. Hayes, M. I. Frecker, and J. H. Adair

The Pennsylvania State University, University Park, PA, 16802, USA

Received: 28 February 2011 – Revised: 27 April 2011 – Accepted: 30 May 2011 – Published: 15 June 2011

Abstract. The fabrication of compliant mechanisms on the mesoscale requires collaboration of mechanical engineering design, with materials science and engineering fabrication approaches. In this paper, a review of current fabrication approaches to produce mesoscale devices is given, highlighting the benefits and limitations of each technique. Additionally, a hierarchy is provided, eliminating fabrication techniques that do not completely satisfy the mechanical design requirements of the compliant mechanisms. Furthermore, the lost mold-rapid infiltration forming process (LM-RIF) is described, and compared to existing fabrication approaches. Finally, prototype mesoscale compliant mechanisms are fabricated, demonstrating the versatility of the LM-RIF process to produce both metal and ceramic devices, as well as ability of a fabrication process to work in collaboration with mechanical design.

1 Introduction

As engineering applications become increasingly complex, the need for collaboration between mechanical engineering design and materials science engineering becomes increasingly apparent. Just as advances in mechanical design have motivated materials scientists to develop new materials with tailored properties, breakthroughs in materials science have, in turn, motivated mechanical engineers to design new and improve existing devices. This exchange of engineering knowledge can be found in the development of almost every present day device and component, ranging from large scale applications such as composite materials used in the automotive and aerospace industries, to small scale applications such as microelectromechanical systems.

In this paper, a collaborative effort between mechanical engineering and materials science engineering is utilized to fabricate and further the development of two mesoscale compliant mechanisms: (1) a compliant forceps for minimally invasive surgery, and (2) a contact-aided compliant cellular mechanism (C3M). In addition, this paper presents the lost mold-rapid infiltration forming (LM-RIF) process, in comparison to other mesoscale fabrication techniques, as a viable mesoscale compliant mechanism fabrication route. This process is based on the initial work of Antolino et al. (2009a, b), to manufacture large arrays of meso-scale devices colloidal science with ultra thick photoresist molding methods.

Correspondence to: G. R. Hayes
(grh144@psu.edu)

2 Micro scale fabrication techniques

Many compliant mechanism designs, such as those designed by Aguirre (2011) and Mehta et al. (2010), result in part sizes on the millimeter scale or larger, with feature sizes on the micrometer scale. While these devices show enhanced performance over traditionally designed devices, the fabrication method used to manufacture the compliant mechanisms needs to be considered. To this end, a summary of fabrication approaches applicable to compliant mechanism device manufacturing have been summarized and explained in this section. The mesoscale is defined in Fig. 1 as a component with dimensions on the millimeter scale with feature sizes on the micrometer scale. The part size and feature size of these mesoscale devices falls between traditional large and small scale fabrication approaches. Therefore, mesoscale compliant mechanisms require new or modified fabrication techniques for successful prototype manufacturing. To date, many microfabrication techniques have been explored to create free standing parts on the mesoscale, consisting of top down, and bottom up approaches (Heule et al., 2003). Top-down approaches consist of processes typical to semi-conductor processing in which, for example, a film is deposited via vapor deposition techniques followed by chemical or reactive ion etching. Additionally, small scale machining technologies, such as direct ceramic machining, wire electrical discharge machining (EDM) (Yan et al., 2004), and low-temperature-co-fired-ceramics machining can cut and grind devices from bulk materials, but can only produce a few parts at a time, generally have significant

Published by Copernicus Publications.

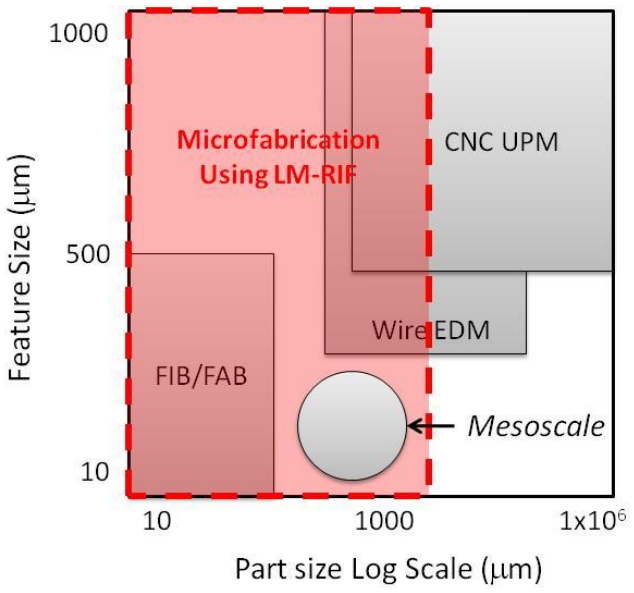

Figure 1. The feature size versus part size comparison are presented for various types of fabrication approaches; focused ion beam and fast atom beam (FIB and FAB), wire electrical discharge machining (Wire EDM), and computer numerical control ultra precision machining (CNC UPM). The lost mold-rapid infiltration forming (LM-RIF) process encompasses the mesoscale while adding the ability to simultaneously manufacture large arrays of parts. The mesoscale lies in the gap in manufacturing size regime above semiconductor fabrication sizes in the sub-10 micron range, and below traditional bulk machining near 300 micron features. Feature size is given on a linear scale, while a logarithmic scale is used to show the wide range in part sizes possible with the fabrication approaches listed.

surface flaws due to the mechanical approach, and yield large quantities of particulate debris (Heule et al., 2003). Machining technologies are also limited by the cutting tool size used to shape the part (Frazier et al., 1995).

Bottom-up techniques consist of the assembly of particulate elements via directed assembly or self-assembly. The additive processes provided by bottom-up approaches are attractive because of a more efficient use of materials and resources, while minimizing manufacturing debris, and avoiding size restrictions due to tool size. Self assembly (Clark et al., 2001) can be used to create arrays of small building blocks, which assemble due to specifically functionalized surfaces, and without the need for external intervention. Alternatively, directed assembly of particulates, via a molding (Muller et al., 2009; Fu et al., 2005), printing (Heule et al., 2003), stereolithography (Heule et al., 2003), or selective laser sintering (Nelson et al., 1995) process can be easily implemented to manufacture devices from a variety of materials available in particulate form. As shown by Bowden and Whitesides (Bowden et al., 1997; Terfort et al., 1997; Xia and Whitesides, 1998), elegant and interesting shapes can be produced with self assembly strategies. The drawbacks of self assembly include arbitrary shape fabrication and the formation of shapes with a substantial thickness (Klajn et al., 2007). Therefore, in the LM-RIF process, directed assembly methods are utilized to form complex particulate bodies with thicknesses of 20 to 300 microns (Antolino, 2010; Antolino et al., 2009a, b).

For directed assembly approaches, there are two main areas of research and development: direct writing methods, and lithography mold-based methods. Direct writing methods, such as direct ink writing (Lewis et al., 2006) of ceramic slurries, do not have the edge control and subsequent edge resolution required for surgical instrumentation, and normally can only fabricate one structure at a time, making these processes relatively inefficient and time consuming. Lost mold processes, such as injection molding of polymer molds (Knitter et al., 2001) and filling of photoresist molds (Schonholzer et al., 2000) offer the ability to create free standing parts large enough, with the desired edge resolution, to be viable options for microfabrication. Furthermore, mold fabrication via lithography is one of the least expensive microfabrication techniques (Lawes, 2007). New advances in ultra thick photoresist techniques permit the fabrication of single layer lithographic molds up to 1mm thick, while maintaining good edge resolution (Lin et al., 2002). Additionally, aqueous gel-casting (Janney et al., 1998; Christian and Kenis, 2007), aqueous tape-casting (Hotza and Greil, 1995), and non-aqueous colloidal suspension formulation (Imbaby and Jiang, 2009), have shown the capability to produce uniform green bodies via colloidal slurries that can be cast into the lithographic molds. Finally, filling photoresist molds with a particulate-based suspension opens the possibilities of processing a wide range of materials including metals, ceramics, composite materials, and multilayer laminated materials. Manufacturing methods for micro components are summarized by Table 1 in terms of smallest feature resolution, aspect ratio, multi-material system capability, and array manufacturing capability. Furthermore, the basis for the technique in terms of lithography, injection molding, machining, printing, and laser forming is used to classify the manufacturing method. To manufacture mesoscale devices, a novel microfabrication process, the LM-RIF, has been developed based on a directed assembly, lost mold method. The LM-RIF process is listed under lithography techniques and outlined in black.

As shown in Fig. 2, multiple fabrication techniques relevant to our objective of large scale manufacturing of mesoscale compliant mechanisms were evaluated and are given in Table 1. To determine the best method of fabrication for compliant mechanisms on the mesoscale, multiple criteria were applied to the possible fabrication approaches listed in Table 1. Fabrication approaches that do not satisfy an applied criterion in the hierarchical diagram are eliminated as viable manufacturing approaches. The applied criteria include: the capability for large array fabrication, high aspect

Table 1. Manufacturing methods for micro components are summarized in terms of smallest feature resolution, aspect ratio, multi-material system capability, and array manufacturing capability. Furthermore, the basis for the technique is used to classify the various methods in terms of lithography, injection molding, machining, printing, and laser forming. The developed LM-RIF process is listed under lithography techniques and outlined in black.

Technique Basis	Micro-Fabrication Method	Smallest Feature Resolution (μm)	Aspect Ratio	2-D or 3-D	Multi-material Systems	Array Capa-bilities	Ref.
Lithography Based Techniques	Micro-fabrica MEMS EFAB	10	high	2-D/3-D	No	Yes	Microfabrica (2010)
	Casting suspensions into photo-lithographic masks on silicon	1–5	1–2	2-D	Yes	Yes	Heule et al. (2003)
	LM-RIF	1–10	1–40	2-D/3-D	Yes	Yes	Antolino et al. (2009a, b)
	Soft lithography	1–5	1–3	2-D/3-D	Yes	Yes	Xia and Whitesides (1998)
	Laminated object manufacturing	100	variable	3-D	Yes	No	Tay et al. (2003)
	Low-temperature co-fired ceramic multilayer	25–100	variable	3-D	No	No	Heule et al. (2003)
	LIGA	10–20	10	2-D	Yes	Yes	Heule et al. (2003)
Injection Molding/ Extrusion	Micro injection molding	20–100	high	3-D	Yes	No	Muller et al. (2009)
	Co-extrusion	5–16	high	3-D	Yes	No	Heule et al. (2003)
	Metal embossing	50	high	2-D	No	No	Heule et al. (2003)
Machining	Direct ceramic machining of pre-sintered bodies	50	variable	3-D	No	No	Heule et al. (2003)
	Microwire EDM	70	high	3-D	No	No	Yan et al. (2004)
	STM-tip electro-chemical etching	0.01	–	2-D	No	No	Heule et al. (2003)
	Precision grinding	50	high	3-D	Yes	No	Heule et al. (2003)
	Diamond machining (lathe)	25	5	3-D	Yes	No	Frazier et al. (1995)
	Surface micro-machining	25	variable	2-D	Yes	No	Frazier et al. (1995)
Printing	Screen printing	100	low	2-D	Yes	Yes	Heule et al. (2003)
	Ink-jet printing of suspensions	70	low	2-D	Yes	No	Heule et al. (2003)
	Freeform ink-jet printing of suspensions	170	high	3-D	Yes	No	Heule et al. (2003)
	3-DP process (printing ceramic binders)	200	variable	3-D	Yes	No	Heule et al. (2003)
	Micropen writing	250	1	3-D	Yes	No	Heule et al. (2003)
Laser Forming	Laser chemical vapor deposition	10	500	3-D	Yes	No	Wanke et al. (1997)
	Pulsed laser ablation	30–200	high	2-D	Yes	No	Heule et al. (2003)
	Micro-stereo-lithography	2	high	3-D	Yes	No	Heule et al. (2003)
	Selective laser sintering	500	high	3-D	Yes	No	Nelson et al. (1995)
	Maple direct write	10–20	low	2-D	No	No	Heule et al. (2003)

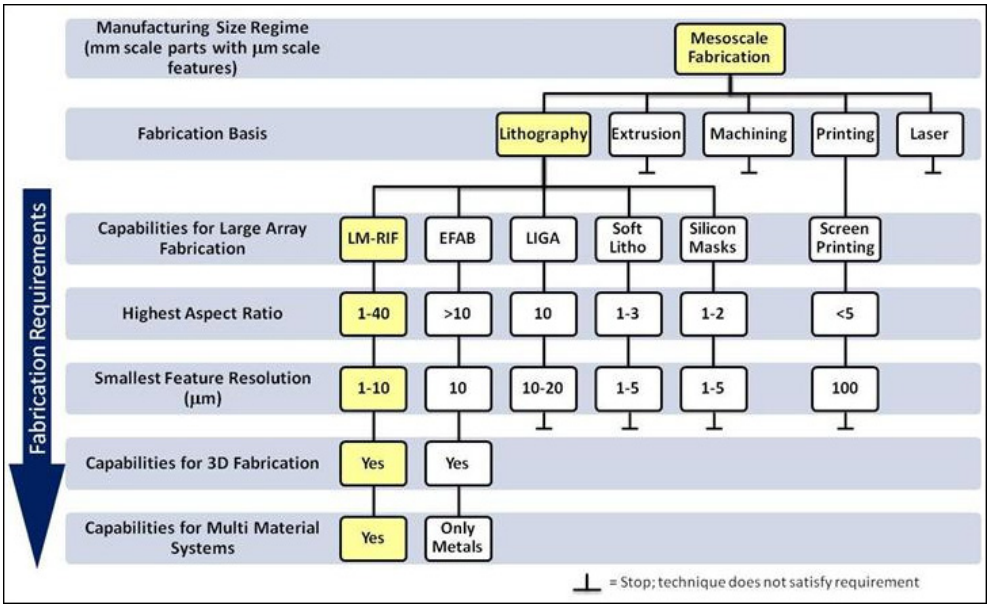

Figure 2. Hierarchy of fabrication techniques used in large array meso-scale manufacturing. Only the LM-RIF process is capable of large array fabrication of 3-D parts with high aspect ratios and small feature resolution, using multiple materials.

ratio in a free standing part, smallest feature resolution, potential for 3-D manufacturing, and capability for multiple material manufacturing. The order of the applied fabrication requirements in Fig. 2 was determined by considering the most desirable fabrication criteria first. To satisfy our objective of large arrays of mesoscale parts manufacturing, the capability for large array manufacturing is the first criterion applied. The remaining criteria were applied in order of importance, as relevant to the prototype devices discussed in Sect. 3.4. It should be noted that changes in the order of the applied requirements in Fig. 2 will result in a change in the ranking of some of the fabrication techniques. However, with all of the fabrication criteria applied, the LM-RIF process will remain the most desirable choice. Meso-scale compliant surgical instruments require components that are 1mm or less in the largest dimension while the feature resolution needs to be at the micron or even sub-micron scale. This requirement eliminates all of the possible microfabrication approaches except the EFAB and LMRIF processes. The EFAB process, invented by Cohen (2002), uses electrochemical deposition of metals combined with lithographic techniques to produce 3-D structures. However, the EFAB process is limited to metallic systems that can be electrochemically deposited. In contrast, the LM-RIF process utilizes nanometer scale ceramic or metallic particulates that in some cases are combined to form ceramic metal composites or ceramic-metal multilayers, permitting a wide range of novel and innovative design strategies. Furthermore, two materials can be combined in a hierarchical fashion, at the particulate scale, in multilayers, and in hybrid material parts in the LM-RIF process.

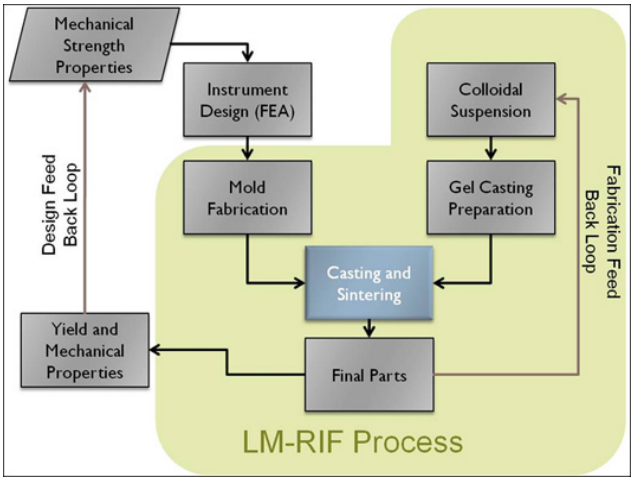

Figure 3. The LM-RIF flowchart. The process starts with a theoretically optimized mechanical design based on initial determination of mechanical properties, followed by mold fabrication, colloidal processing, and final part fabrication. Final parts are tested and characterized, with the mechanical properties used to design changes in the design and fabrication for future generations of materials and/or design components. Changes in the design geometry of the part are completed through the Design Feedback loop, while changes to the manufacturing process and material system are completed through the Fabrication Feedback loop.

3 The Lost Mold-Rapid Infiltration Forming Process (LM-RIF)

The LM-RIF process, illustrated in Fig. 3, consists of an integrated, iterative approach to both improve the mechanical design of the part being manufactured; via the design feedback loop, as well as improve the fabrication process itself; via the fabrication feedback loop that optimizes material mechanical properties. The LM-RIF process and manufacturing approach has been developed over multiple generations to improve both the basic material properties and component geometry. Antolino et al. describes the basic approach to improve material properties based on the manufacture of three mole percent yttria zirconia polycrystalline (3YTZP) mesoscale bend bars that are $15\times20\times370$ microns in dimension (Antolino et al., 2009a, b). However, in these preliminary reports, neither larger parts that can completely bridge the manufacturing gap in Fig. 1 into the 1 mm regime while maintaining micron scale features nor additional materials that expand the design space were reported. The innovations required to meet these challenges will be highlighted in this process overview section.

As illustrated in Figs. 3 and 4, the process begins with an initial compliant mechanism design based on both size and topology optimization techniques (Mehta, 2010; Aguirre and Frecker, 2007; Mehta et al., 2009; Aguirre, 2011). Once the first generation design is finalized, a lithography-based mold fabrication step is used to translate the design into a two or three dimensional mold. After molds are fabricated, a concentrated colloidal suspension (i.e., 40 to 50 volume percent solids) is formulated using the precursor particulate materials. The colloidal suspension is then cast into the mold via a screen printing squeegee, and solvent is removed by evaporation under carefully controlled conditions to minimize capillary forces to prevent part cracking. Final parts are obtained after a combined mold removal and sintering step. The finished parts are characterized, and appropriate changes can be made to the mechanical design, colloidal suspension parameters, or both to optimize components in subsequent generations. Through this process development, the ability to produce large arrays of parts from both metals and ceramics, as well as parts ranging in thickness from 10 to 400 microns has been demonstrated (Aguirre, 2011).

3.1 Mold fabrication

The optimal compliant mechanism design approach (Aguirre and Frecker, 2007; Mehta, 2010; Mehta et al., 2009, 2010), is used to generate a photomask. In this process, the prototype parts are arranged in a layout to facilitate a high volume of parts fabricated per unit area, while satisfying part proximity constraints. The separation distances among parts, also known as the proximity of parts, on the mask layout is determined via the designed mold thickness, with a 1:1 ratio of mold thickness to inter-part spacing. While each patterned part on the photomask is designed for a particular mold thickness, it is possible to have single photomasks with multiple sections designed for various part thickness.

In the mold fabrication process, polished polycrystalline, high purity (greater than 99.5 weight per cent) alumina substrates (courtesy of Kyocera Corporation or Coorstek) are used as substrates to avoid handling components between processing steps. SU8 (Microchem Corp.) photoresist molds are fabricated on the substrates using a modified UV lithography process. Initially, an antireflective coating of AZ-Barli-II 90 is spin coated onto the substrate to eliminate mold defects created by light scattering from the substrate surface. Secondly, a 10 μm under layer of SU-8 photoresist is spin coated to form the bottom layer of the mold. This under layer assures part separation from the substrate before sintering and acts as a smooth, flat bottom surface for the mold. Finally, a SU-8 layer with the targeted thickness is deposited using a calculated volume technique adapted from Lin et al. (2002) In this process, a known volume of SU-8 photoresist is deposited at 80 °C onto a substrate of specific surface area. The photoresist is prebaked at 120 °C for 4 h, with a temperature ramp of 2 °C per minute, during which the solvent is evaporated from the resist, and self leveling takes place. Next, an initial optical exposure of 3 mJ cm^{-2} micron^{-1} (thickness) is performed. The photoresist then undergoes a post exposure bake at 55 °C for 30 min with a temperature ramp of 2 °C per minute, and finally the resist is developed for 30 min with slight agitation. The mold layer is developed in propyleneglycol monomethyletheracetate (PGMEA, SU-8 Developer, Microchem Corp.). Following development, one of two additional mold manufacturing paths can be taken. For a single layer (i.e., two dimensional molds and subsequent components), a second flood exposure of approximately 4200 mJ cm^{-2} in concert with an additional heat treatment at 180 °C for 20 min fully crosslinks the resist. Alternatively following development, two or more mold layers can be laminated at 100 °C with slight pressure (0.01 MPa). The process of stacking and laminating multiple mold layers can be used to create three dimensional mold cavities and, as a consequence, more complex, three dimensional components. During the exposure steps, a UV light filter (Omega Optical, PL-360-LP) ensures vertical side walls in the final mold (del Campo and Greiner, 2007). Figure 4a shows the UV lithography layering sequence, as well as the steps going from design, to mask, to final mold cavity. In Fig. 4a, a cross sectional view of mold cavities is shown with varying length and width. It is noted that as mold thickness increases, minimum feature size increases. The minimum, stand alone, single feature size for the parts fabricated herein was taken to be approximately 1/15 of the mold thickness, while inherent features of larger part geometries can be as small as 2–3 μm (Yang and Wang, 2005).

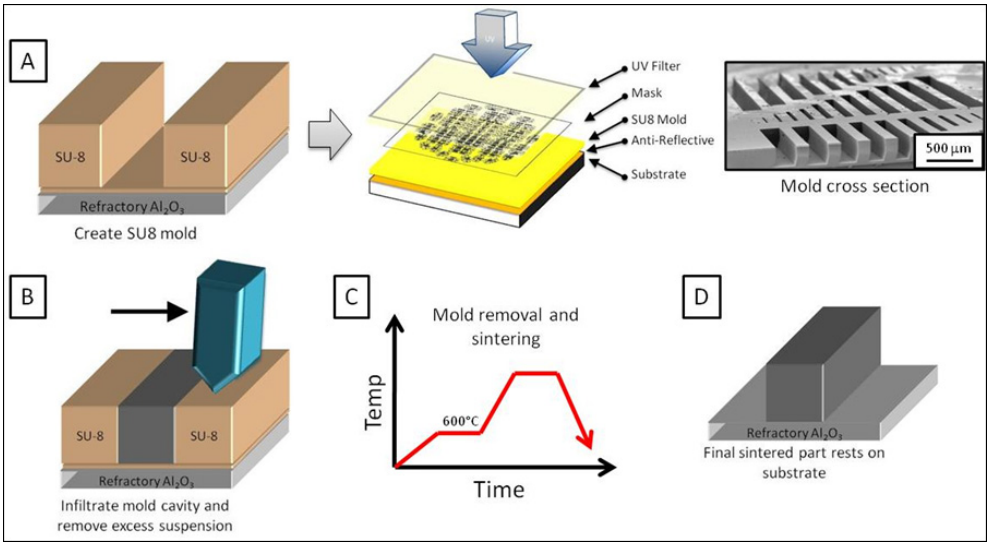

Figure 4. The LM-RIF process steps of mold fabrication, infiltration, mold and binder removal and sintering are depicted. **(A)** Molds are fabricated on high purity refractory substrates via a modified lithography technique. The lithography stack is shown, along with a cross sectional scanning electron micrograph of a sample mold. **(B)** The fabricated molds are then infiltrated with a high solids loading colloidal suspension via a screen printing squeegee and allowed to dry. **(C)** The mold and binder in the colloidal suspensions is removed at 600 °C, followed by sintering, forming a dense final part. The specific furnace cycle is as follows: In ambient atmosphere, ramp 2 °C min^{-1} to 600 °C and hold 2 h. In an atmosphere of 5 vol% H_2 and 95 vol% N_2, ramp 5 °C min^{-1} to 1300 °C, hold 2 h, and cool at 10 °C min^{-1}. **(D)** freestanding parts are left on the original substrate.

3.2 Colloidal suspension formulation

Well dispersed, high solid loading suspensions are required during particulate processing to fabricate dense parts with desired mechanical integrity. The properties of the particulate that is being processed, including particle size distribution, shape, and chemistry, can affect the processing parameters used to create a colloidal suspension. In particular, the high density from uniform particle packing of well-dispersed particulate has a positive influence on the sintering of the particulate body (Reed, 1995). Likewise, poorly packed particulates from poorly dispersed, agglomerated particulates results in poorly sintered materials with trapped porosity, grain growth and other characteristics that compromise mechanical properties (Reed, 1995). Thus, the particulate processing characteristics ultimately influence the final mechanical properties of components. If the processing parameters create colloidal suspensions with solids content too low, agglomerated particulates or other particulate created defects, the packing density in green state is compromised, and sintering to high density, to achieve mechanically strong parts, will not take place. Conversely, desired mechanical properties dictate processing parameters used to create suitable colloidal suspensions from particulates. If the desired mechanical strength is relatively low, and/or a porous final body is required for a particular application, the processing parameters can be modified to fit these requirements. The topology of the compliant mechanism design also affects the processing parameters, as intricate designs may require special processing parameters. Finally, whether mechanical properties are dictated through design, or measured through experimentation, the design will need to be modified to fit within the given system. Principally, as well as in the context of the LM-RIF process, powder processing parameters, mechanical properties, mechanical design, and initial powder properties are interrelated aspects of powder processing. Variation in each of these attributes directly influences the others, and thus, when working to improve the system as a whole, the impact of changes in one attribute must be evaluated for all other aspects. For example, properties of the particulate material being incorporated into the LM-RIF process, such as particle size, particle shape, agglomeration characteristics, density, and chemical stability, play a direct role in the processing parameters utilized, such as solvent environment, colloidal dispersion scheme, drying method, binder removal, and sintering. Furthermore, the properties of particulates, both alone, and in conjunction with the processing parameters have direct impacts on mechanical properties and mechanical design of fabricated devices. Additionally, compliant mechanism design can dictate a specific material property, such as biocompatibility, high elastic modulus, or even desired feature size. These specifications influence the starting material powder material type and particle size, as well as desired mechanical properties, and can even constrain processing parameters. The interaction of some processing parameters, such as sintering temperature, on mechanical properties, has been described by Antolino (2010). Therefore, it

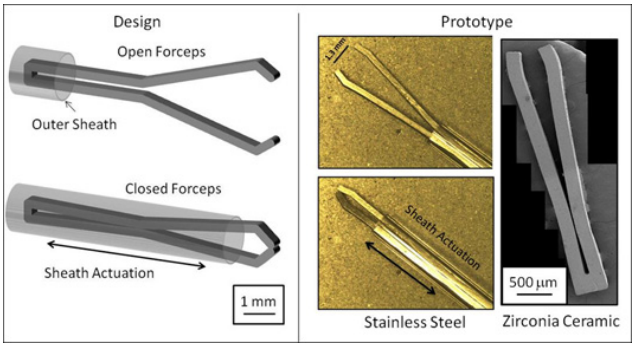

Figure 5. (Left) The design of the compliant forceps device is shown. The forceps is actuated via a sheath, a grasping action is obtained via moving the sheath forward, forcing the arms toward one another. (Right) Stainless steel prototype forceps are shown in an optical image, as fabricated by the LM-RIF process. The actuation of the forceps is shown in both the open and closed positions. Additionally, zirconia ceramic forceps are shown in a scanning electron micrograph, as fabricated by the LM-RIF process. The stainless steel and zirconia forceps demonstrate the ability of the LM-RIF process to fabricate prototype compliant mechanisms from multiple materials.

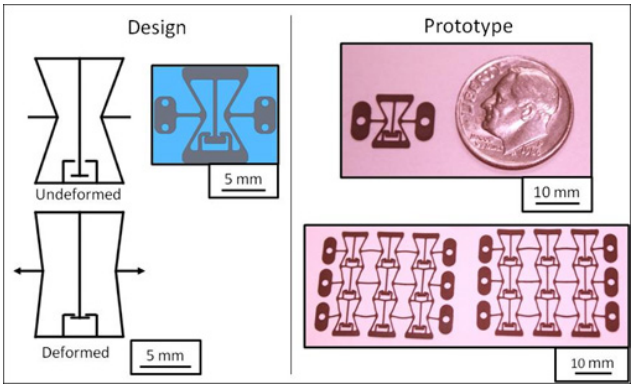

Figure 6. (Left) The design of contact-aided compliant cellular mechanisms is shown in both the undeformed and deformed cases. As the mechanism is deformed, contact occurs in the dash-pot structure, resulting in a distribution of stresses throughout the device, allowing further elastic deformation. The final design is shown in blue. (Right) Optical images of prototype designs of the C3M devices, as fabricated by the LM-RIF process are shown for both a single unit cell, and a 3×3 cellular array. A US Dime is shown for scale reference. The stainless steel parts demonstrate the ability of the LM-RIF process to fabricate mesoscale compliant mechanism devices.

is clear that the system of interactive particle processing must be considered as a whole, without eliminating the impact of one area on another.

3.3 Mold removal and sintering

During the infiltration process, an excess of suspension is placed on top of the mold and worked into the mold cavities with a squeegee while simultaneously removing any bubbles. Following infiltration and drying, the green parts are sintered in a two stage process. Initially, the mold is removed by thermolysis in the ambient, air atmosphere at 600 °C. After demolding takes place, the free standing parts are sintered in an appropriate atmosphere and temperature and time. The specific furnace cycle is as follows: mold removal in ambient atmosphere, ramp 2 °C min^{-1} to 600 °C and hold 2 h. Sintering in an atmosphere of 5 vol% H_2 and 95 vol% N_2, ramp 5 °C min^{-1} to 1300 °C, hold 2 h, and cool at 10 °C min^{-1}. Figure 4b–d depicts the casting, burnout and sintering steps leaving final parts freestanding on the original substrate.

Following fabrication, free standing parts can be evaluated for mechanical properties, as well as device functionality. As shown in Fig. 3, changes to the design, as well as changes to the colloidal processing formulations can be made through the appropriate feedback loops, permitting fine tuning of the LM-RIF process.

3.4 Fabrication of prototypes

Prototype mesoscale devices, consisting of a surgical forceps and contact aided compliant cellular mechanisms, were successfully fabricated utilizing the LM-RIF process. Example prototype compliant forceps devices are shown in Fig. 5. The forceps are dimensionally on the mesoscale due the centimeter length scale of the forceps arms, with micrometer length scale of the gap between the forceps arms. During actuation, a sheath moves over the forceps arms, forcing them together in a grasping action. The arms come into contact with one another during grasping, distributing stresses within the arms and allowing further elastic deformation. The prototyped devices were tested in concurrent studies by Aguirre (Aguirre, 2011; Aguirre et al., 2011) and Addis (2010). Performance testing was carried out by experimentally and theoretically correlating the tip deflection of the forceps as a function of the displacement of the sheath. It was found that the finite element analysis is able to accurately predict the onset of plastic deformation of the forceps during actuation. Good agreement between the theoretical and experimental results verified the device's performance and the design and manufacturing procedure. Secondly, a pre-clinical tool assessment procedure was conducted by Addis (2010) at Penn State Hershey Medical Center (Hershey, PA, USA), which compared the performance of the prototypes against a commercially available product (Boston Scientific 1mm diameter Spybite® biopsy forceps). It was found that the prototype instrument was preferred over the standard instrument in terms of the ability to control intermediate positions between the open and closed positions of the jaws, and the prototype instrument's ability to grasp firmly is superior to that of the standard instrument. Positive feedback validated the

surgical relevance of the device and provided valuable insight for improving the next generation of prototypes (Addis et al., 2011).

Example contact-aided compliant cellular mechanisms are shown in Fig. 6. These cellular mechanisms are designed to maximize horizontal elastic strain, while maintaining high stiffness. When actuated in the horizontal direction, the auxetic cell deforms, allowing for large elastic strain. Furthermore, during deformation, the dash-pot mechanism comes into contact, distributing stresses in the walls of the C3M device, allowing further elastic deformation. These C3M devices fall into the mesoscale due to the centimeter scale of the unit cell, millimeter size scale of the length of the oblique walls, and the micrometer size scale of the dash-pot contact mechanism. In a concurrent study by Mehta et al. (2009), the force and global elastic strain of the C3M devices were experimentally determined by conducting a force-deflection analysis using a force gauge actuated by a micrometer. It was found that the elastic modulus of the meso-scale stainless steel C3M parts fabricated using LM-RIF process is between 70 to 150 GPa, and that the global strain is sensitive to the size and quality of the contact gap. Good agreement was found between the theoretical and experimental global elastic strain of the C3M devices fabricated with the LM-RIF process.

Truly mesoscale parts can be fabricated using the LM-RIF process. Additionally, while just a few examples of metallic and ceramic parts are shown, these parts were manufactured in large arrays of similar parts, demonstrating the manufacturing capability of the LM-RIF process.

4 Conclusions

The collaboration between mechanical design and materials science fabrication has been described within the context of two mesoscale devices: a surgical forceps instrument, and C3M device. The possible fabrication methods for these devices have been described, listing the benefits and drawbacks of each technique. In addition to existing techniques, a new fabrication technique, the LM-RIF, was introduced and included in the comparison. Furthermore, a hierarchy was developed to easily choose the fabrication technique most applicable to the devices in question. The LM-RIF fabrication process was described that can; (1) fabricate large arrays of compliant mechanisms; and (2) be complementary to particulate based material systems. Furthermore, using this manufacturing technique for both surgical instrument and C3M device design is attractive because free standing parts are fabricated with the desired large aspect ratios while retaining good resolution on the micron scale stemming from the lithographic based molds and colloidal infiltration processes. Both zirconia ceramic and stainless steel components were manufactured with the LM-RIF process to emphasize the range of materials possible with the fabrication approach.

In concurrent studies, prototype surgical forceps devices and C3M devices were mechanically evaluated and good agreement was found between the experimental results and calculated performance.

Future extensions and improvements to the LM-RIF process, and the supporting materials science research fall into the following categories: (1) Manufacturing of multilayer, or three dimensional structures. To date, multi-layering using the described mold fabrication technique in Sect. 3.1 has been demonstrated with a 2 layer mold. Future work involves utilizing the multilayer molds to manufacture multilayer devices. (2) Improving device performance through the incorporation of two or more materials in one device layer. (3) Additional testing of the mechanical properties of the metal, ceramic, and composite components via theta-test specimens and tensile test specimens.

Acknowledgements. The work in this manuscript is partially funded under NSF STTR 0637850, NSF 0900368, and NSF 0437214, the NSF I/UCRC Ceramic and Composite Materials Center. This work was also supported by the Pennsylvania State University Materials Research Institute Nanofabrication Network and the National Science Foundation Cooperative Agreement No. 0335765, National Nanotechnology Infrastructure Network, with Cornell University. Any opinions, findings, and conclusions or recommendations expressed in this publication are those of the author(s) and do not necessarily reflect the views of Cornell University nor those of the National Science Foundation. The authors also gratefully acknowledge the partial support provided by grant number R21EB006488 from the National Institute of Biomedical Imaging And Bioengineering. The content in this paper is solely the responsibility of the authors and does not necessarily represent the official views of the National Institute of Biomedical Imaging And Bioengineering or the National Institutes of Health.

Edited by: J. Andrés Gallego Sánchez
Reviewed by: two anonymous referees

References

Addis, M.: Evaluation of Surgical Instruments for Use in Minimally Invasive Surgery, B.S. Honor Thesis, Department of Mechanical and Nuclear Engineering, The Pennsylvania State University, University Park, PA, 2010.

Addis, M., Aguirre, M., Frecker, M., Haluck, R. S., Mathew, A., Pauli, E. M., and Gopal, J.: Development of Tasks and Evaluation of a Prototype Forceps for NOTES, JSLS-J. Soc. Laparoend., under review, 2011.

Aguirre, M.: Design and Optimization of Narrow-Gauge Contact-Aided Compliant Mechanisms for Advanced Minimally Invasive Surgery, Doctor of Philosophy Mechanical Engineering, The Pennsylvania State University, University Park, 2011.

Aguirre, M. and Frecker, M.: Size and Shape Optimization of a 1.0 mm Multifunctional Forceps-Scissors Surgical Instrument, ASME Journal of Medical Devices, 2, 015001-015001-015001-015007, 2007.

Aguirre, M. E., Hayes, G., Meirom, R., Frecker, M., Muhlstein, C., Adair, J. H., and Kerr, J. A.: The Design and Fabrication of

Narrow-Gauge (1 mm Diameter) Surgical Instruments for Natural Orifice Translumenal Endoscopic Surgery, J. Mech. Design, accepted, 2011.

Antolino, N. E.: Lost Mold-Rapid Infiltration Forming: Strength Control in Mesoscale 3Y-TZP Ceramics, Doctor of Philosophy, Materials Science and Engineering, The Pennsylvania State University, University Park, 2010.

Antolino, N. E., Hayes, G., Kirkpatrick, R., Muhlstein, C. L., Frecker, M. I., Mockensturm, E. M., and Adair, J. H.: Lost Mold Rapid Infiltration Forming of Mesoscale Ceramics: Part 1, Fabrication, J. Am. Ceram. Soc., 92, S63–S69, doi:10.1111/j.1551-2916.2008.02627.x, 2009a.

Antolino, N. E., Hayes, G., Kirkpatrick, R., Muhlstein, C. L., Frecker, M. I., Mockensturm, E. M., and Adair, J. H.: Lost Mold-Rapid Infiltration Forming of Mesoscale Ceramics: Part 2, Geometry and Strength Improvements, J. Am. Ceram. Soc., 92, S70–S78, doi:10.1111/j.1551-2916.2008.02719.x, 2009b.

Bowden, N., Terfort, A., Carbeck, J., and Whitesides, G. M.: Self-assembly of mesoscale objects into ordered two-dimensional arrays, Science, 276, 233–235, 1997.

Christian and Kenis, P. J. A.: Fabrication of ceramic microscale structures, J. Am. Ceram. Soc., 90, 2779–2783, doi:10.1111/j.1551-2916.2007.01840.x, 2007.

Clark, T. D., Tien, J., Duffy, D. C., Paul, K. E., and Whitesides, G. M.: Self-assembly of 10-mu m-sized objects into ordered three-dimensional arrays, J. Am. Chem. Soc., 123, 7677–7682, 2001.

Cohen, A. L.: Method for Electrochemical Fabrication, USA Patent, US 6 475 369 B1, 2002.

del Campo, A. and Greiner, C.: SU-8: a photoresist for high-aspect-ratio and 3D submicron lithography, J. Micromech. Microeng., 17, R81–R95, doi:10.1088/0960-1317/17/6/r01, 2007.

Frazier, A. B., Warrington, R. O., and Friedrich, C.: The Miniaturization Technologies – Past, Present, and Future, IEEE Trans. Ind. Electron., 42, 423–430, 1995.

Fu, G., Loh, N. H., Tor, S. B., Tay, B. Y., Murakoshi, Y., and Maeda, R.: Injection molding, debinding and sintering of 316L stainless steel microstructures, Appl. Phys. A-Mater., 81, 495–500, doi:10.1007/s00339-005-3273-6, 2005.

Heule, M., Vuillemin, S., and Gauckler, L. J.: Powder-based ceramic meso- and microscale fabrication processes, Adv. Mater., 15, 1237–1245, 2003.

Hotza, D. and Greil, P.: Aqueous tape casting of ceramic powders, Mater. Sci. Eng. A-Struct. Mater. Prop. Microstruct. Process., 202, 206–217, 1995.

Imbaby, M. F. and Jiang, K.: Stainless steel-titania composite micro gear fabricated by soft moulding and dispersing technique, Microelectron. Eng., 87, 1650–1654, 2009.

Janney, M. A., Omatete, O. O., Walls, C. A., Nunn, S. D., Ogle, R. J., and Westmoreland, G.: Development of low-toxicity gelcasting systems, J. Am. Ceram. Soc., 81, 581–591, 1998.

Klajn, R., Bishop, K. J. M., Fialkowski, M., Paszewski, M., Campbell, C. J., Gray, T. P., and Grzybowski, B. A.: Plastic and moldable metals by self-assembly of sticky nanoparticle aggregates, Science, 316, 261–264, 2007.

Knitter, R., Gohring, D., Risthaus, P., and Hausselt, J.: Microfabrication of ceramic microreactors, Microsyst. Technol., 7, 85–90, 2001.

Lawes, R. A.: Manufacturing costs for microsystems/MEMS using high aspect ratio microfabrication techniques, Microsyst. Technol., 13, 85–95, 2007.

Lewis, J. A., Smay, J. E., Stuecker, J., and Cesarano, J.: Direct ink writing of three-dimensional ceramic structures, J. Am. Ceram. Soc., 89, 3599–3609, doi:10.1111/j.1551-2916.2006.01382.x, 2006.

Lin, C. H., Lee, G. B., Chang, B. W., and Chang, G. L.: A new fabrication process for ultra-thick microfluidic microstructures utilizing SU-8 photoresist, J. Micromech. Microeng., 12, 590–597, 2002.

Mehta, V.: Design, Analysis, and Applications of Cellular Contact-Aided Compliant Mechanisms, Doctor of Philosophy, Mechanical Engineering, The Pennsylvania State University, University Park, 2010.

Mehta, V., Frecker, M., and Lesieutre, G. A.: Stress Relief in Contact-aided Compliant Cellular Mechanisms, ASME J. Mech. Des., 31, 1–11, 2009.

Mehta, V., Hayes, G. H., Frecker, M. I., and Adair, J. H.: Design, Fabrication, and Testing of Meso-scaled Cellular Contact-aided Compliant Mechanisms, ASME 2010 Conference on Smart Materials, Adaptive Structures and Intelligent Systems, SMASIS2010, Philadelphia, Pennsylvania, USA, 28 September–1 October 2010, 2010.

Microfabrica Inc.: http://www.microfabrica.com/, last access: December 2010.

Muller, T., Piotter, V., Plewa, K., Guttmann, M., Ritzhaupt-Kleissl, H. J., and Hausselt, J.: Ceramic micro parts produced by micro injection molding: latest developments, Microsyst. Technol., 16, 1419–1423, doi:10.1007/s00542-009-0992-1, 2009.

Nelson, J. C., Vail, N. K., Barlow, J. W., Beaman, J. J., Bourell, D. L., and Marcus, H. L.: Selective Laser Sintering of Polymer-Coated Silicon-Carbide Powders, Ind. Eng. Chem. Res., 34, 1641–1651, 1995.

Reed, J. S.: Principles of ceramics processing, Wiley & Sons, 1995.

Schonholzer, U. P., Hummel, R., and Gauckler, L. J.: Microfabrication of ceramics by filling of photoresist molds, Adv. Mater., 12, 1261–1263, 2000.

Tay, B. Y., Evans, J. R. G., and Edirisinghe, M. J.: Solid freeform fabrication of ceramics, Int. Mater. Rev., 48, 341–370, 2003.

Terfort, A., Bowden, N., and Whitesides, G. M.: Three-dimensional self-assembly of millimetre-scale components, Nature, 386, 162–164, 1997.

Wanke, M. C., Lehmann, O., Muller, K., Wen, Q. Z., and Stuke, M.: Laser rapid prototyping of photonic band-gap microstructures, Science, 275, 1284–1286, 1997.

Xia, Y. N. and Whitesides, G. M.: Soft lithography, Annu. Rev. Mater. Sci., 28, 153–184, 1998.

Yan, M. T., Huang, C. W., Fang, C. C., and Chang, C. X.: Development of a prototype Micro-Wire-EDM machine, J. Mater. Process. Tech., 149, 99–105, doi:10.1016/j.jmatprotec.2003.10.057, 2004.

Yang, R. and Wang, W. J.: A numerical and experimental study on gap compensation and wavelength selection in UV-lithography of ultra-high aspect ratio SU-8 microstructures, Sens. Actuator B-Chem., 110, 279–288, 10.1016/j.snb.2005.02.006, 2005.